

# Application of impregnated biocarbon produced from soybean hulls in dye decolorization

Aleksandra Kulić Mandić, Milena Bečelić Tomin, Gordana Pucar Milidrag, Milena Rašeta and Đurđa Kerkez

Faculty of Sciences, University of Novi Sad, Department of Chemistry, Biochemistry and Environmental Protection, 21000 Novi Sad, Serbia

## Abstract

Waste soybean hulls (WSH) were investigated as a Fe-support in two forms: raw and carbonized (*i.e.* biocarbon, BC), as possible value-added materials. Fe-impregnation was implemented in order to produce heterogeneous Fenton catalysts for Reactive Blue 4 dye degradation. Materials characterization demonstrated a rise in the specific surface area due to decomposition of WSH constituents during carbonization (to obtain BC) and thermal activation (to obtain Fe-WSH and Fe-BC), thus producing catalysts with high mesoporosity and hematite as the active site for Fenton reaction. Among the investigated materials, Fe-WSH showed the greatest ability for  $\cdot\text{OH}$  production in acidic medium. Next, the heterogeneous Fenton process was optimized by using response surface methodology, which resulted in selection of the following reaction conditions: 3 mM  $\text{H}_2\text{O}_2$ , 100 mg Fe-WSH, reaction time of 180 min, at a constant pH 3, RB4 concentration of 50 mg  $\text{dm}^{-3}$  and at room temperature. The achieved dye removal and mineralization were 85.7 and 66.8 %, respectively, while the catalyst showed high stability and the reaction intermediates formed during the oxidation process had a low inhibitory effect on *Vibrio fischeri* bacteria.

**Keywords:** valorization; Fe(III)-impregnation; response surface methodology; Reactive Blue 4; reuse.

Available on-line at the Journal web address: <http://www.ache.org.rs/HI/>

ORIGINAL SCIENTIFIC PAPER

UDC: 66.099.72:676.87:  
(662.734+582.736.308)

Hem. Ind. 75 (5) 307-320 (2021)

## 1. INTRODUCTION

Textile industry has a highly demanding production in terms of water, chemicals and energy consumption. Only in cotton dyeing process more than 100 L of fresh water is used per 1 kg of textile, where unfixed reactive dyes (up to 50 % of the initial concentration) end up in wastewaters [1,2]. The dye presence in water bodies has a highly negative influence on aquatic organisms [3]. For example, Reactive Blue 4 (RB4) dye, which is commonly used, shows acute toxicity to fish [4]. Structurally, RB4 consists of a dichlorotriazine group and anthraquinone chromophore. Due to its high water solubility and low biodegradability, wastewater treatment is required in processes using this dye [5,6].

Advanced oxidation processes (AOPs), based on radical generation with significant redox potential, can non-selectively degrade dye aromatic structures. Among many AOPs, the heterogeneous Fenton process is emphasized due to simple operation, wide application range and successful pollutant oxidation [7–12]. As biological treatments are commonly used in textile industry, Fenton reaction can be implemented as a pre- or post-technique in the hybrid wastewater treatment.

Synthesis of active, stable, and reusable catalyst is a top concern for researchers. An overview of various support materials used as catalysts in heterogeneous Fenton reaction was given in recent review studies [7,9,13]. Some of the mostly used are clays, zeolites, activated carbon, silicates and biosorbents. A common method for catalyst preparation is

---

Corresponding author: Milena Bečelić-Tomin, Faculty of Sciences, Department of Chemistry, Biochemistry and Environmental Protection, 21000 Novi Sad, Serbia

E-mail: [milena.becelic-tomin@dh.uns.ac.rs](mailto:milena.becelic-tomin@dh.uns.ac.rs)

Paper received: 27 April 2021; Paper accepted: 12 August 2021; Paper published: 1 October 2021.

<https://doi.org/10.2298/HEMIND210427023K>



wet impregnation [14], which is accomplished in two steps: (1) dispersion of the metal precursor onto the support surface and in the interparticle space and (2) thermal activation in order to modify the surface and texture of the raw material [3,15,16].

With the growth of human population, production of agricultural solid waste is on rise [17]. From a circular economy point of view, it is important to support additional uses of low-quality agricultural by-products and turn them into valuable resources, thus supporting cascading of materials as long as possible [18]. Carbonization is commonly used in order to prepare porous biocarbon materials for application in wastewater treatment [19,20]. Recently, Fenton-like application of such materials (fruit shells, straws, *etc.*) was reviewed [21].

One of the possible waste streams that can be used in such manner is soybean hulls. In Serbia, production of soybean is on a constant rise and data show yield of 806407 t in 2020 [22], which ranks Serbia among countries with the highest average yield in Europe. Waste soybean hulls (WSH) account for 7-8 % of the total soybean mass [23,24]. Some of the investigated applications of WSH are: ethanol and bio-oil production, animal feed [24], fermentable sugars [25], cellulose nanofibers [26], cellulose pulp [23], energy source by pyrolysis [27], activated carbon production [28] and adsorption in wastewater treatment [24]. Still, it could be seen that WSH have not been studied as a catalyst support raw material yet.

The focus of this work was to test bio-waste (soybean hulls) value addition as a Fenton catalyst support in the process of RB4 dye decolorization. For this purpose, thermal (carbonization) and chemical (Fe-impregnation) treatments of WSH were performed. Effects of the waste modification were confirmed by using different methods (Brunauer-Emmett-Teller (BET) method, scanning electron microscopy coupled with energy dispersive spectrometry (SEM/EDS), Fourier-transform infrared (FTIR) spectroscopy and X-ray diffraction (XRD) analysis). Optimization of dye decolorization was conducted by using response surface methodology (RSM). Central composite design (CCD) was used to simultaneously investigate effects of selected factors and to interpret the results using a statistical model. Dye degradation products, effluent toxicity, catalyst stability and reusability were monitored.

## 2. MATERIALS AND METHODS

All chemicals were used as obtained without purification. RB4 (CAS 13324-20-4, dye content  $\geq 35$  %, molecular formula:  $C_{23}H_{14}Cl_2N_6O_8S_2$ ),  $Fe(NO_3)_3 \cdot 9H_2O$  ( $\geq 98$  %),  $Na_2CO_3$  ( $\geq 99.5$  %),  $H_2O_2$  (30 %, w/w), 95–97 %  $H_2SO_4$ , catalase from bovine liver (CAS 9001-05-2), methanol ( $\geq 99.9$  %) were purchased from Sigma-Aldrich (USA). All solutions were prepared with deionized water (DI). WSH were kindly provided by a soybean processing company with the industrial capacity of 250,000 t per year (AP Vojvodina, Serbia). Upon the receipt raw WSH were ground to the 0.3 mm fraction.

### 2. 1. Catalyst preparation

Two materials were used as Fe-catalyst supports: raw and carbonized WSH. The biowaste carbonization was conducted at 550 °C for 4 h in a muffle furnace with the aim to produce biocarbon (BC).

In our previous work [29] we tested the improved Fe-impregnation method with the use of ultrasound (US) waves in order to shorten the required time for catalyst preparation. In that case, bentonite clay was used as the Fe-support. In the present work, the optimal parameters from this procedure were applied: the  $Fe^{3+}$ /material ratio of 3 mmol  $g^{-1}$ , the suspension exposure to US waves during impregnation and the calcination temperature of 350 °C. Firstly, the support material suspension (1 g in 50  $cm^3$  DI) was mixed for 30 min. Then, the impregnation precursor (55  $cm^3$  of 0.2 mol  $dm^{-3}$   $Fe(NO_3)_3 \cdot 9H_2O$  solution was mixed with powdered  $Na_2CO_3$  at the molar ratio of  $[Na^+]/[Fe^{3+}]=1$ ) was sonicated for 5 min (20 kHz and 10 % amplitude; Ultrasonic Homogenizer Sonopuls HD 2200, Bandelin, Germany). The processed Fe-precursor was added drop-by-drop to the material suspension and US was applied for 10 min. The impregnated WSH or BC were dried in a water bath (100 °C) and washed several times with DI water. After drying and calcination (350 °C, 2 h), the samples were labeled as Fe-WSH and Fe-BC.

### 2. 2. Characterization methods

WSH, BC, Fe-WSH and Fe-BC were subjected to the structural analysis by the Autosorb iQ Surface Area Analyzer (Quantachrome Instruments, USA), after sample degassing (105 °C). Specifically, the multi-point BET (Brunauer-Emmett-

Teller) method was used for determination of the specific surface area; BJH (Barrett-Joyner-Halenda), HK (Horvath-Kawazoe) and total pore volume (TPV) methods were used for determination of pore volume and size measurements (average pore radius, APR). Scanning electron microscopy (SEM) (TM3030, Hitachi High-Technologies, Japan) coupled with energy dispersive spectrometry (EDS) (Bruker Quantax 70 X-ray detector system, Bruker Nano, Germany) was used for the morphological analysis. The KBr pellet method was used for Fourier Transform infrared spectroscopy (FTIR) at a Thermo-Nicolet Nexus 670 spectrophotometer (USA) (4000-400  $\text{cm}^{-1}$  range in a diffuse reflection mode at a 4  $\text{cm}^{-1}$  resolution). A Rigaku MiniFlex 600 (USA) diffractometer with  $\text{CuK}\alpha$  radiation (scanning range was  $5 < 2\theta < 80^\circ$  with 0.03° step) was used for X-ray diffraction analysis.

### 2. 3. Heterogeneous Fenton process

Control experiments of WSH, BC, Fe-WSH and Fe-BC application in sorption and the heterogeneous Fenton process were conducted under the following conditions: 100 mg of the prepared material was added to 100  $\text{cm}^3$  of RB4 solution (50  $\text{mg dm}^{-3}$ ). pH value was set to 3 with the use of diluted  $\text{H}_2\text{SO}_4$  (WTW inoLab pH/ION 735, Germany). The Fenton reaction was initiated with 10 mM  $\text{H}_2\text{O}_2$  (in sorption tests this step was left out). After 180 min of reaction, the mixture was filtered through a 0.45  $\mu\text{m}$  membrane filter. Decolorization efficiency was determined by using a UV-Vis spectrophotometer (UV-1800, Shimadzu, Japan) at  $\lambda_{\text{max}}=597.5$  nm. Stability of the materials was monitored by inductively coupled plasma-mass spectrometry (ICP-MS; Agilent Technology, Japan) as the total Fe content leached in the aqueous phase (EPA 6020B).

Central composite design (CCD) was employed to investigate decolorization efficiency as a response to 3 independent factor variations (Design-Expert 12 software-trial version; Stat-Ease Inc., USA). Examined variable ranges were selected based on literature review [6, 16, 30], and are presented in Table 1. 20 probe runs were created, including 6 replications of central levels. Analysis of variance (ANOVA) was used for further statistical analysis to identify interactions between selected variables and the response. Verification of the chosen model and optimal reaction conditions was performed by 5 confirmation runs.

Table 1. Experimental conditions and levels of independent variables ( $c_{\text{H}_2\text{O}_2}$  -  $\text{H}_2\text{O}_2$  concentration,  $m_{\text{catalyst}}$  - catalyst mass,  $t$  - reaction time) according to CCD

Code	Variable	Level ( $\alpha$ )				
		$-\alpha$	-1	0	+1	$+\alpha$
A	$c_{\text{H}_2\text{O}_2}$ / mM	0.6	3.0	6.5	10.0	12.4
B	$m_{\text{catalyst}}$ / mg	33	50	75	100	117
C	$t$ / min	19	60	120	180	221

The optimal setting for the heterogeneous Fenton reaction was used for further kinetics analysis (0; 15; 30; 45; 60; 80; 100; 120; 150; 180 min). Decolorization efficacy and content of leached Fe were determined according to before mentioned procedures. Degree of RB4 mineralization was measured as the total organic carbon (TOC, LiquiTOC Elementar II, Japan) according to EPA 415.3 method. Evaluation of inhibitory effect on *Vibrio fischeri* bacteria (LUMISTox 300, Dr Lange, Germany; ISO 11348-1:2008) was conducted with freshly prepared bacteria suspension and after scavenging residual  $\text{H}_2\text{O}_2$  by catalase solution [31] in all samples. NaCl was added in order to reach 20  $\text{g dm}^{-3}$ , pH value (6.5-8) and concentration of dissolved  $\text{O}_2$  ( $>3$   $\text{mg dm}^{-3}$ ) were measured before testing. Sample inhibition was calculated from the luminescence intensity before and after sample addition to *V. fischeri* suspension. The impact of  $\cdot\text{OH}$  on the reaction efficiency was determined in the test with methanol as a radical scavenger (0.1 M MeOH was added before oxidant). Also,  $\cdot\text{OH}$  scavenging capacity (RSC) was measured according to the modified method reported in literature [32], after 15 min of reaction. Degradation products were analyzed by gas chromatography–mass spectrometry (GC-MS, Agilent 7890A/5975C, Japan), where EPA 3510C method was used for sample preparation and the manufacturer's method for determination of non- and semi-polar compounds. The reusability test was conducted 5 times under optimal reaction conditions (catalyst was washed with DI and dried (105 °C) after each use).

### 3. RESULTS AND DISCUSSION

#### 3. 1. Characterization study

Characterization of surface characteristics of both impregnated as well as the initial support materials was conducted by conventional methods to evaluate differences based on the modification path and future application possibilities.

BET method was employed for an indication of changes in textural features (Table 2). Low values of the surface area and the total pore volume as well as high average pore radius are obtained for WSH, which was expected due to the macroporous hulls nature. Balint *et al.*, [33] have indicated that carbonization and impregnation processes lead to an increase in porosity as a result of decomposition of the WSH cellular structure. Similar results were obtained in the present study. An increase in the surface area of biocarbon was observed from 0.3 to 11 m<sup>2</sup> g<sup>-1</sup>. The impregnation process had further pronounced effect on micro- and mesopore volume, where a significant TPV rise, and APR reduction indicate appearance of mesoporous surfaces of the prepared catalysts (Fe-WSH and Fe-BC). The surface area expanded to 55 and 104 m<sup>2</sup> g<sup>-1</sup>, respectively. The mechanical effect of ultrasound (microjets and shock waves) during modification can be responsible for breakdown of the catalyst support to smaller particles [34]. Thus, a larger surface area is available for Fe(OH)<sub>3</sub> precipitation during impregnation. Thermal activation at 350 °C had an important part in generating active and mesoporous catalysts, where hematite crystals may be produced.

Table 2. Textural features of investigated materials

Material	Surface area, m <sup>2</sup> g <sup>-1</sup>	Micropore volume by HK, cm <sup>3</sup> g <sup>-1</sup>	Mesopore volume by BJH, cm <sup>3</sup> g <sup>-1</sup>	APR, nm	TPV, cm <sup>3</sup> g <sup>-1</sup>
WSH	0.3	not detected	0.001	67.10	0.001
BC	11	0.004	0.054	9.76	0.056
Fe-WSH	55	0.022	0.177	6.32	0.174
Fe-BC	104	0.042	0.425	8.00	0.416

Surface topology was investigated by SEM and the obtained micrographs are presented in Figure 1. WSH has clear and well-ordered fibrous hull forms consisting of palisade (the outer epidermal layer of tightly packed macrosclereids) and hourglass cells (the hypodermal layer of osteosclereids with expanded ends). These anatomic hull parts are made of cellulose, hemicellulose and pectin (insoluble carbohydrates) and they are bound together with lignin [23]. The drastic influence of carbonization (Fig. 1b) resulted in a porous, “fluffy” appearance of residual ash. Further, the impregnation process (Fe ions incorporation and thermal activation) led to noticeable morphological changes of both WSH and BC (Figs 1c and d). A high number of irregularly shaped Fe-doped particles appeared on both materials. These aggregates differ in size, where Fe-WSH has generally rough particles of approximately 25 μm in size, while Fe-BC retained similar surface characteristics as biocarbon with many smaller particles. Validation of these strong, visual changes in WSH after modification can be linked with presented data on the increases in the surface area and mesopore volume (Table 2).

Elemental composition was quantified by the EDS method (Fig. 2). High O and C content (~46 wt.%) in WSH was foreseen due to the hull structure (Fig. 1a). Besides, Ca, K and Al (3.6, 3.0 and 1.0 wt.%, respectively) were also detected. Increase in K and Ca fractions, and appearance of Mg, Si, P and S in BC are connected to the main carbonization effect, destruction of organic matter that is followed by the release of gases, as reported in literature [27]. It is assumed, that this is the reason for the decrease in C and O contents after carbonization and thermal treatment in BC, Fe-WSH and Fe-BC samples. Moreover, the main impact of impregnation on WSH was replacement of Ca and K with high Fe content (66.9 wt.%). The simultaneous processes of Fe-(hydr)oxide transformation and WSH decomposition, led to production of a Fe-rich solid catalyst. Further, EDS also indicates successful impregnation of BC samples. The formed Fe-oxide resulted in an increase in Fe (19.5 wt.%) and O (38.4 wt.%) contents in Fe-BC. The difference in Fe contents after impregnation can relate to the porosity and average pore radius in support materials (Table 2). Namely, Fe diffusion during ultrasound impregnation was conditioned by the microporous WSH structure and mesopore enriched structure of BC. Additionally, the C percentage has risen to 9.0 wt.% after another thermal treatment of Fe-BC, which may be related to possible char production [33]. Ash like composition of Fe-BC (Fig. 1d) is partially preserved (Ca = 25; Mg = 4.0; Al, Si, P and K < 2 wt.%).

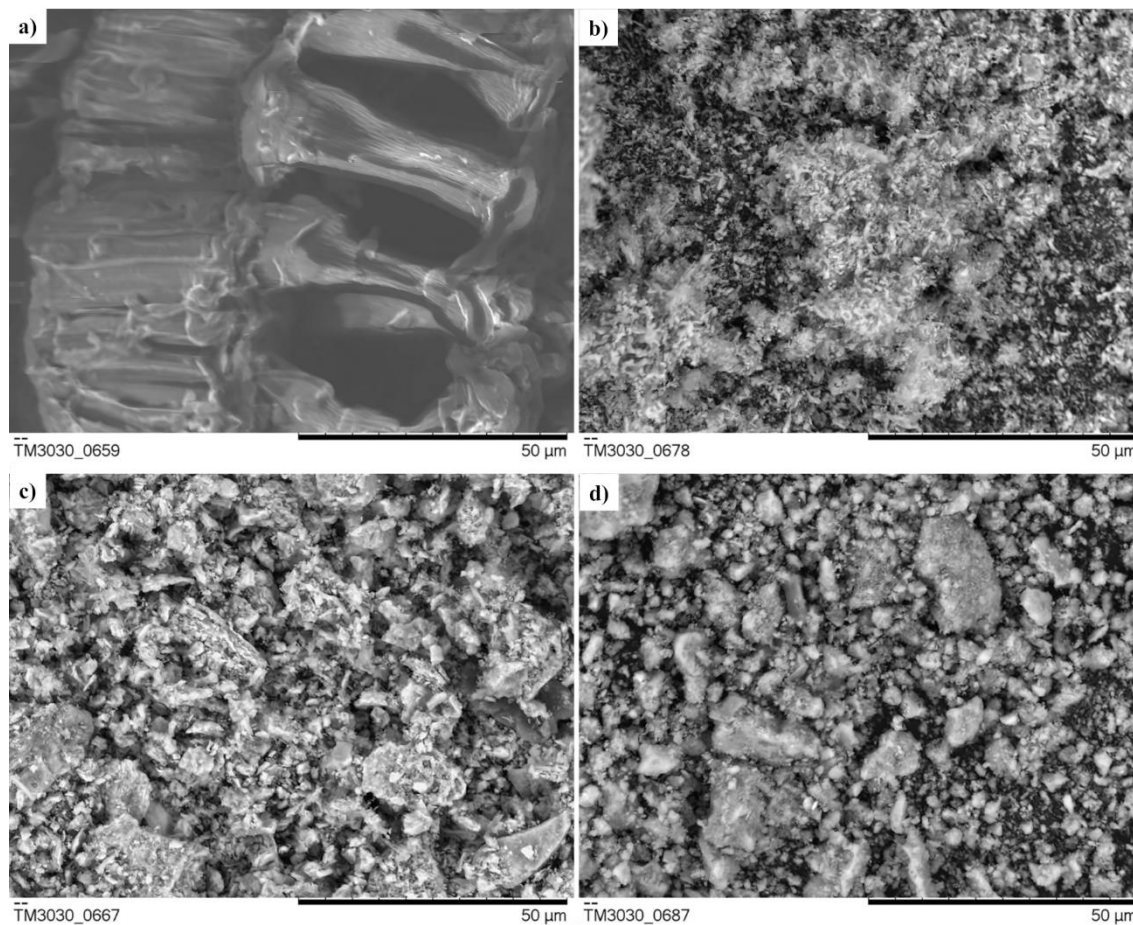


Fig. 1. SEM micrographs of: a) WSH, b) BC, c) Fe-WSH and d) Fe-BC

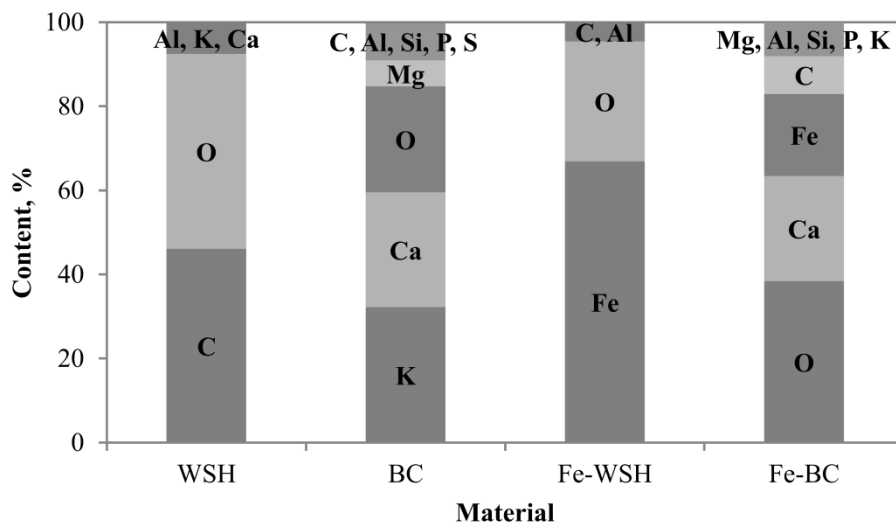


Fig. 2. Elemental composition by the EDS analysis of all investigated materials

Further confirmation of the WSH structure was obtained by the IR spectrum where the highest intensity band ( $3410\text{ cm}^{-1}$ ) represents OH stretching vibrations of cellulose and moisture in the biomass. Also, two peaks at  $\sim 2900\text{ cm}^{-1}$  are associated with vibrations of CH and  $\text{CH}_2$  asymmetrical stretching in hemicellulose. The peak at  $1739\text{ cm}^{-1}$  is attributed to acetyl ester groups in hemicellulose and/or phenyl ester group between lignin and hemicellulose. Besides, the lignin aromatic ring (C=C) stretching is associated with  $1645\text{ cm}^{-1}$  peak and CO stretching of cellulose ( $1035\text{ cm}^{-1}$ )

[26]. Carbonization induced lower BC surface functionality. The most prominent band is assigned to carbonate ion and has two peaks at 1460 and 876  $\text{cm}^{-1}$  [35], which is in accordance with the obtained ash like surface (Fig. 1b and Fig. 2). When comparing to WSH, the reduction in intensity and small shift of peaks associated with OH (3440  $\text{cm}^{-1}$ ), CH, CH<sub>2</sub> (2916, 2850  $\text{cm}^{-1}$ ) and CO stretching (1057  $\text{cm}^{-1}$ ) are identified. WSH impregnation (Fe-WSH) leads to a significant increase in Fe content (Fig. 2) that produced two, strong intensity peaks of characteristic FeO stretching vibration (544, 453  $\text{cm}^{-1}$ ). OH (3404  $\text{cm}^{-1}$ ), C=C (1629  $\text{cm}^{-1}$ ) and CO (1049  $\text{cm}^{-1}$ ) vibrations are also present, but as less notable peaks. IR spectra of Fe-BC, additionally indicates the increase in the biocarbon yield shown by SEM/EDS, where carbonate ion peaks are prominent (1456, 874  $\text{cm}^{-1}$ ). CO stretching (1054  $\text{cm}^{-1}$ ) and OH vibrations (3427  $\text{cm}^{-1}$ ) have a higher intensity than the initial support (BC). While comparing impregnated materials, broad, medium intense absorption in the range 550-400  $\text{cm}^{-1}$  could be assigned to FeO vibration. The difference between Fe-BC and Fe-WSH peak intensity in this IR region, further confirm the impregnation process outcome (EDS; Fig. 2).

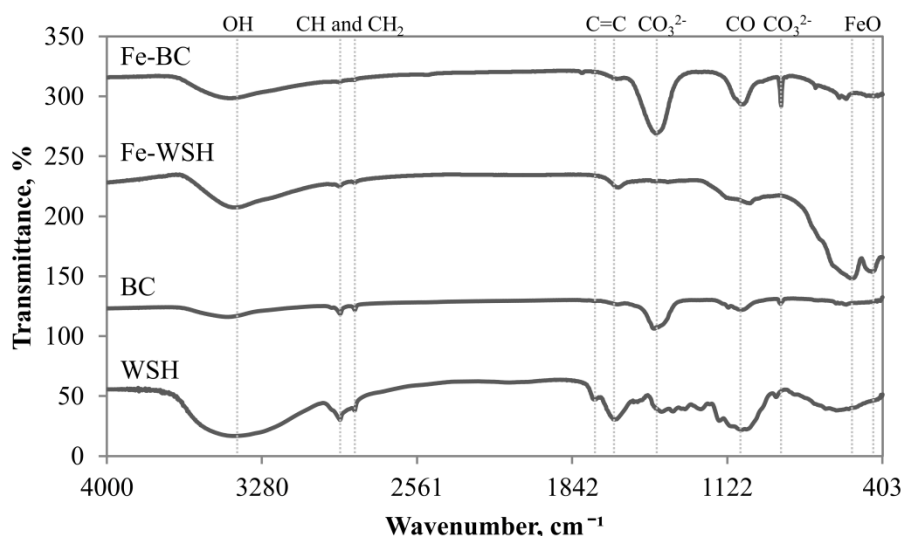


Fig. 3. FTIR spectra of all investigated materials with characteristic functional groups

XRD diffractogram profiles are shown in Figure 4. WSH shows a semicrystalline pattern with one crystalline peak ( $2\theta = 34.6^\circ$ ) and broad, amorphous humps ( $2\theta = 13-25^\circ$ ). Namely, peaks at  $2\theta = 17.3^\circ, 20.5^\circ, 22.3^\circ$  and  $34.6^\circ$  are typical for type I cellulose, which is the most abundant native crystalline polymorph form [24]. With either modification (BC, Fe-WSH, Fe-BC), a semicrystalline pattern of WSH becomes crystalline due to the breakage of amorphous hull fractions (cellulose, hemicellulose). BC diffractogram shows many peaks, related to CaCO<sub>3</sub> (PDF 00-005-0586;  $2\theta = 23.1, 29.4, 36.1, 39.4, 42.9, 47.4, 48.5$  and  $60.5^\circ$ ), Al<sub>2</sub>O<sub>3</sub> (PDF 00-010-0173;  $2\theta = 25.9, 35.3$  and  $41.6^\circ$ ) and SiO<sub>2</sub> (PDF 00-046-1045;  $2\theta = 26.5, 40.3$  and  $50.3^\circ$ ) while the peak with the highest intensity at  $27.9^\circ$  was due to fairchildite mineral (K<sub>2</sub>Ca(CO<sub>3</sub>)<sub>2</sub>; PDF 00-900-8300;  $2\theta = 13.2, 19.4, 33.9, 44.4$  and  $48.1^\circ$ ). Diffraction peaks found after impregnation (Fe-WSH) correspond to hematite (PDF 00-033-0664), at angles  $2\theta = 24.2, 33.2, 35.7, 40.9, 49.5, 54.1, 62.7$  and  $64.0^\circ$ . The same phase was detected in Fe-BC, with a slightly shifted peak ( $2\theta = 32.7^\circ$ ), while the rest of the pattern is linked to CaCO<sub>3</sub> already identified as the main phase in carbonized WSH. In our work, both impregnated materials show crystalline patterns in contrary to the results reported by Chen *et al.*, [36], where corn husk retained amorphous pattern after similar processes. The average Fe<sub>2</sub>O<sub>3</sub> crystal size was 26.2 nm (Fe-WSH) and 23.8 nm (Fe-BC) based on the Scherrer's formula [37], that confirms the thermal transformation of Fe-hydroxide to oxide at 350 °C.

All applied methods induced significant changes in surface morphology and chemistry after WSH modification. According to BET and SEM data, the surface area and porosity significantly expanded, while the other characterization methods confirmed the presence of Fe after impregnation. Namely, the retained ash like structure and increased surface area of Fe-BC, provide a basis for application of this material in the sorption process. On the other hand, Fe-WSH has the potential to be used as a Fenton reaction catalyst due to high Fe content. These assumptions are important for subsequent dye solution treatment.

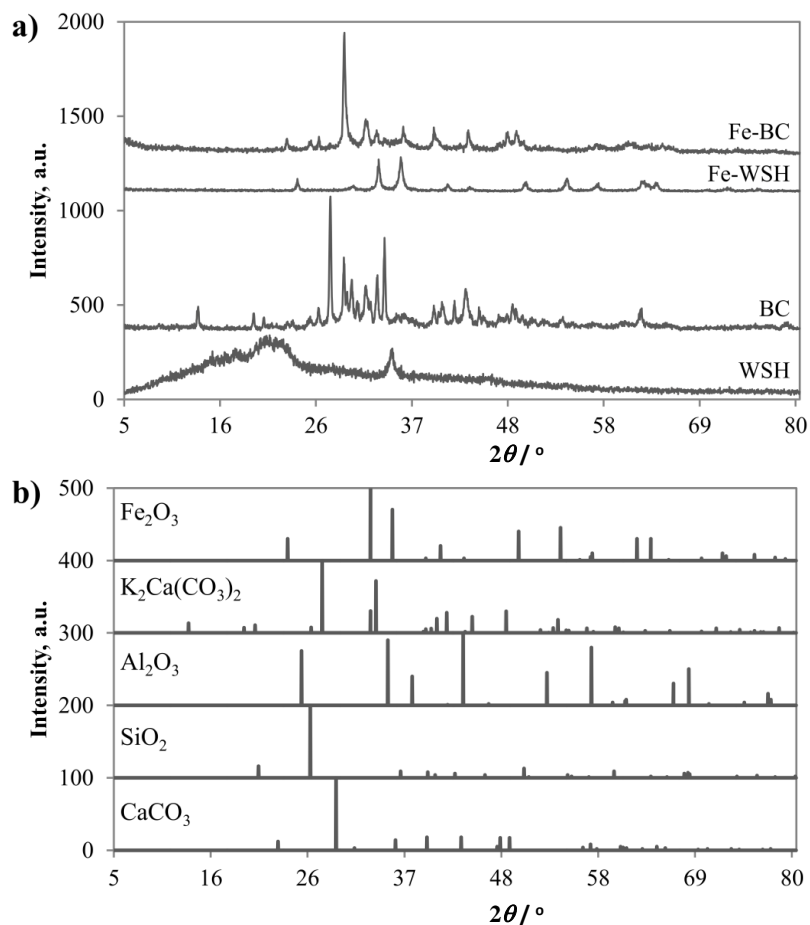


Fig. 4. XRD analysis: a) XRD diffractogram of four materials and b) PDF card peak patterns

### 3. 2. Application of biocarbon materials in dye decolorization

In order to understand decolorization of RB4 by the heterogeneous Fenton process using modified soybean hull biocarbon samples, control experiments were conducted (Fig. 5). A series of tests were performed at a pH 3 as optimal for the Fenton reaction. It is important to indicate that RB4 is anionic in nature in either acidic or alkaline medium [38].

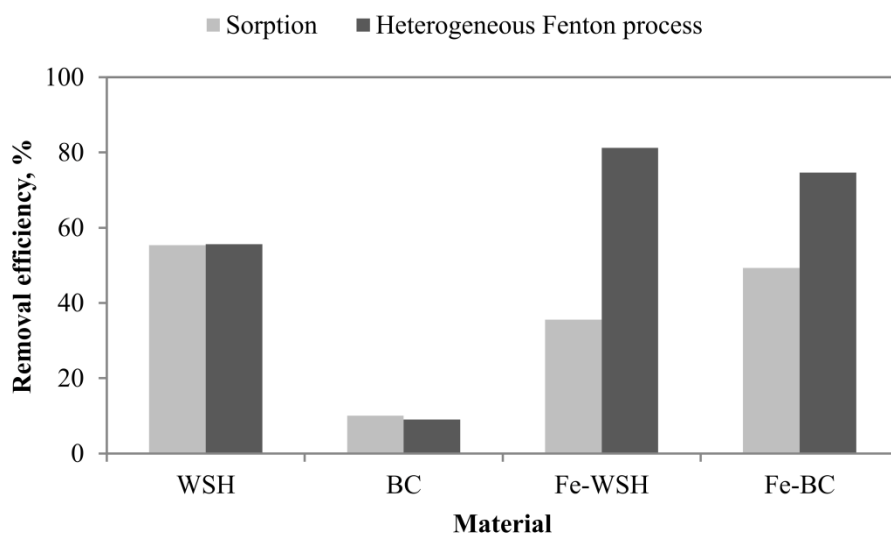


Fig. 5. Control experiments (adsorption and oxidation of RB4 dye solution) with the investigated materials. Reaction conditions:  $c_{RB4} = 50 \text{ mg dm}^{-3}$ ;  $V_{RB4} = 100 \text{ cm}^3$ ; pH 3;  $m_{material} = 100 \text{ mg}$ ;  $c_{H_2O_2} = 10 \text{ mM}$ .



In both, sorption and Fenton processes, WSH exhibited a moderate RB4 removal, probably due to macroporosity and Fe absence. The carbonized material (BC) had the lowest activity, even though it had the increased surface area. The presence of Ca, K, Mg, Al (proved by EDS, XRD), may induce the alkaline surface as oxides of these metals are known strong bases [36]. After the pH adjustment, significant change in net surface charge is possible and therefore electrostatic repulsion of RB4 molecules is occurring. The presented BC nature and absence of transition metals, able to initiate the Fenton reaction, are the reason for the obtained RB4 removal of only 10 %.

In comparison to BC, dye sorption was improved with Fe-WSH and Fe-BC. It is assumed that the higher Fe content in Fe-WSH may be associated to the presence of many positively charged sites, able to electrostatically attract RB4 as compared to Fe-BC. Since the presence of Fe species was confirmed, the increased activity of impregnated catalysts in the Fenton process was not surprising. Namely, 81.3 and 74.7 % dye was removed with Fe-WSH and Fe-BC, respectively. The reason is the reaction between  $\equiv\text{Fe}_2\text{O}_3$  and adsorbed  $\text{H}_2\text{O}_2$ . Electronic transfer results in the ferric complex ( $\equiv\text{Fe}-\text{OOH}^{2+}$ ) formation and its further decomposition to  $\cdot\text{OOH}$  and  $\equiv\text{Fe}^{2+}$ , that leads to production of desired  $\cdot\text{OH}$  radicals [3, 39]. Additionally, the material stability is also an important factor. Measured Fe leaching varied depending on the applied material and type of the process. During the dye sorption test,  $0.77 \text{ mg dm}^{-3}$  (Fe-WSH) and  $0.64 \text{ mg dm}^{-3}$  (Fe-BC) of total Fe was detected in solution due to favored reaction between  $\equiv\text{Fe}_2\text{O}_3$  and  $\text{H}^+$  under acidic conditions. In the Fenton process,  $\text{H}_2\text{O}_2$  decomposition results in higher catalyst stability, where Fe-WSH shows a lower leaching potential ( $0.13 \text{ mg dm}^{-3}$ ) than Fe-BC ( $0.39 \text{ mg dm}^{-3}$ ).

Given the importance of the efficiency of the material preparation method (required time, energy consumption) and the effectiveness of the Fenton process (percentage of the removed dye, catalyst stability), further optimization study of RB4 decolorization process was performed with Fe-WSH.

### 3. 3. Fe-WSH in the Fenton process – RSM optimization study

RSM was implemented to optimize  $A - c_{\text{H}_2\text{O}_2}$ ,  $B - m_{\text{Fe-WSH}}$  and  $C -$  reaction time to obtain a satisfying RB4 decolorization efficiency. The CCD matrix (factorial, *central*, *star* points) and removal efficiencies are presented in Table 3. As CCD is used for building a second order model, the backward stepwise regression of a quadratic model ( $\alpha = 0.1$ ) was implemented to find a reduced model that best explains the results. Adequacy of the reduced model was tested by the analysis of variance (ANOVA) by tests of the significance of regression model with individual model coefficients and lack of fit test.

Table 3. CCD design matrix and experimental results

Standard order	Run order	Factor A $c_{\text{H}_2\text{O}_2} / \text{mM}$	Factor B $m_{\text{Fe-WSH}} / \text{mg}$	Factor C $t / \text{min}$	Efficiency, %	
					Actual response	Predicted response
15	1	6.5	75	120	70.7	62.6
8	2	10.0	100	180	79.5	80.6
16	3	6.5	75	120	62.5	62.6
9	4	0.6	75	120	70.5	66.9
4	5	10.0	100	60	67.0	66.4
3	6	3.0	100	60	75.3	71.5
5	7	3.0	50	180	55.7	58.8
11	8	6.5	33	120	40.1	40.1
14	9	6.5	75	221	75.9	74.5
6	10	10.0	50	180	52.0	53.7
20	11	6.5	75	120	59.9	62.6
12	12	6.5	117	120	82.1	85.2
10	13	12.4	75	120	58.8	58.3
19	14	6.5	75	120	61.4	62.6
2	15	10.0	50	60	39.8	39.6
17	16	6.5	75	120	66.8	62.6
7	17	3.0	100	180	80.4	85.7
13	18	6.5	75	19	44.0	50.7
1	19	3.0	50	60	42.3	44.7
18	20	6.5	75	120	67.6	62.6

ANOVA, the fit and model comparison statistics and final equation provided by the backward elimination for decolorization prediction (in coded factors) are shown in Table 4. The results show the model significance ( $p$ -value  $< 0.05$ ) with the main, linear effects of  $A$ ,  $B$  and  $C$ , while the two-level interaction and second-order effects are not significant ( $p$ -value  $> 0.1$ ).  $p$ -values for these coefficients were:  $C^2 = 0.1138$ ,  $B^2 = 0.1734$ ,  $BC = 0.4554$ ,  $AC = 0.5667$ ,  $AB = 0.8018$  and  $A^2 = 0.9213$ . It was found that both  $m(\text{Fe-WSH})$  and reaction time were the most significant factors for the RB4 decolorization. Obtained  $R^2$  value (0.9289) is high, and indicates that the 92.9 % of the data variability is explained by the reduced model. Variation of the predicted data shown as the predicted  $R^2$  (0.8937) is in good agreement with the adjusted  $R^2$  (presents variation of the experimental data). High values of  $R^2$ , adjusted  $R^2$  and predicted  $R^2 \sim 0.9$  also indicate validation of the model. Additionally, the adequate precision value measures the range of the predicted data to the average prediction error. The desirable signal to noise ratio is larger than 4 with the adequate precision of 26.2 obtained with the reduced model indicates an adequate signal.

Table 4. ANOVA results for reduced central composite design, fit and model comparison statistics and final equation in terms of coded factors

Source	Sum of squares	df	Mean square	F-value	p-value	
Model	3232	3	1077	69.67	<0.0001	significant
A	89.34	1	89.34	5.778	0.0287	
B	2458	1	2458	159.0	<0.0001	
C	684.6	1	684.6	44.27	<0.0001	
Residual	247.4	16	15.46			
Lack of Fit	159.7	11	14.52	0.828	0.6330	not significant
Pure Error	87.72	5	17.54			
Cor Total	3479	19				
Std. Dev.	3.932		$R^2$	0.9289		
Mean	62.61		Adjusted $R^2$	0.9156		
Coefficient of Variance	6.280		Predicted $R^2$	0.8937		
			Adeq. Precision	26.22		

Decolorization efficiency, % = 62.61 - 2.56 A + 13.42 B + 7.08 C

The main diagnostics plot is the normal probability of residuals (Fig. 6a), which reveals that errors are distributed normally and that there is a straight-line pattern of residuals. This finding supports the adequacy of the least-squares fit, which indicates the use of the proposed model for heterogeneous Fenton process optimization.

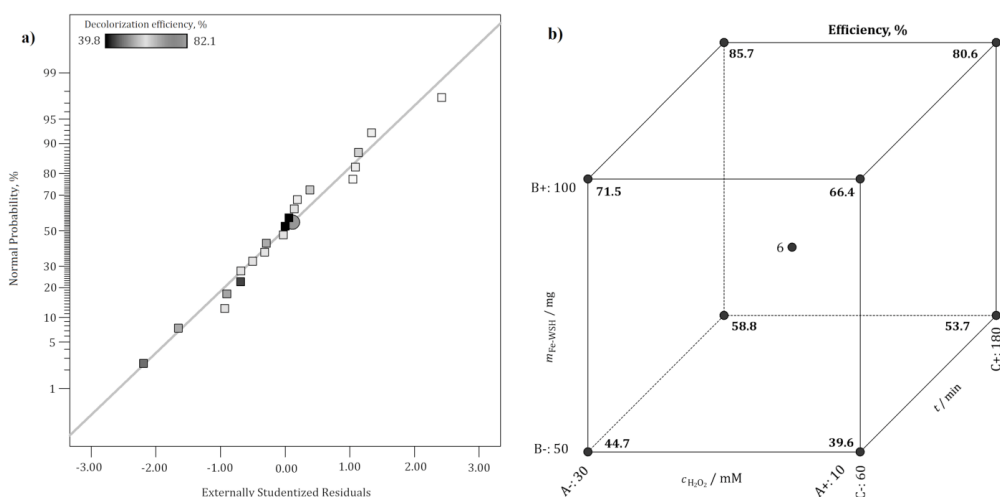


Fig 6. Diagnostic plot: a) normal probability vs. externally studentized residuals; Model graph: b) cube plot of predicted decolorization efficiency (A-left and right; B-up and down; C-front and back faces)

The cube plot (Fig. 6b) displays the three investigated factors variation outcomes in one place. Axes present three factors from in the range from low to high and coordinate points are predicted dye removals of factorial probes (Table 3). Oxidant concentration is an important factor for treatment efficacy [3,7,9] and the RSM analysis indicated that the

lowest  $\text{H}_2\text{O}_2$  concentration was optimal. It is assumed that reaction between 3 mM  $\text{H}_2\text{O}_2$  and 100 mg Fe-WSH provided an adequate amount of  $\cdot\text{OH}$  radicals for RB4 decolorization (85.7 %). Higher oxidant amounts reduced the process efficiency, due to production of less active hydroperoxylic radicals ( $\cdot\text{OOH}$ ) and  $\text{H}_2\text{O}$  [30]. Similar outcome was observed in literature [40] in the Fenton reaction between pyrite ash and RB4 dye, where 99.5 % removal was achieved with the initial  $\text{H}_2\text{O}_2$  concentration of 4 mM. Moreover, the influence of Fe-WSH dose is important and beneficial for dye removal by heterogeneous Fenton reaction. Due to the catalyst increased dose and generally high surface area, mesoporosity and hematite crystals as active sites, adsorption and catalytic decomposition of  $\text{H}_2\text{O}_2$  can occur simultaneously thus positively affecting treatment outcome. In a review paper on factors that affect catalytic activity the reaction time was stressed as an important parameter for achieving complete dye degradation [10]. Prolonged operation provides sufficient time for heterogeneous Fenton reagents to react. The reaction time has a positive and linear effect, where RB4 decolorization efficiency increased as the reaction time increased from 19 to 221 min (Table 3).

Overall, the desired goal of RSM was to optimize the RB4 decolorization efficiency. The predicted removal was 85.7 % and desirability function 0.762. The optimal reaction conditions were: 3 mM  $\text{H}_2\text{O}_2$ , 100 mg Fe-WSH, and reaction time of 180 min. The model verification test confirmed good correlation with the observed decolorization efficiency 85.2 % (mean value) with low standard deviation (1.8 %) in 5 consecutive runs.

### 3. 4. Evolution of RB4 mineralization

Heterogeneous Fenton optimal conditions were kept constant in the period from 5-180 min for determination of the reaction kinetics. Results depicted in Figure 7 show RB4 removal and mineralization, together with methanol  $\cdot\text{OH}$  scavenging and *Vibrio fischeri* inhibition of the effluent during the reaction.

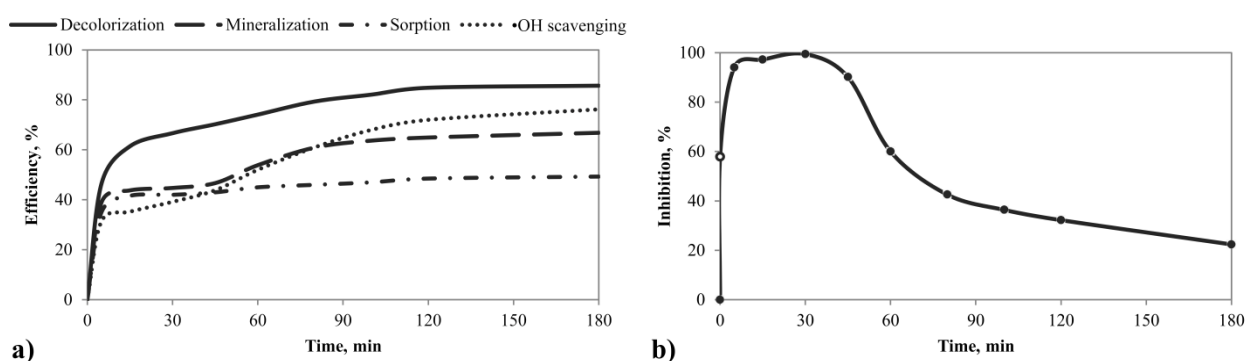


Fig. 7. Kinetics of RB4 oxidation: a) heterogeneous Fenton process performance and b) effluent acute toxicity on *V. fischeri* bacteria. Reaction conditions:  $c_{\text{RB4}}=50 \text{ mg dm}^{-3}$ ;  $V_{\text{RB4}}=100 \text{ cm}^3$ ;  $\text{pH } 3$ ;  $m_{\text{material}}=100 \text{ mg}$ ;  $c_{\text{H}_2\text{O}_2} = 3 \text{ mM}$

The highest rise in RB4 decolorization efficiency was detected in the first 15 min (from 46.6 to 61.4 %) with an intensifying effect up to 100 min (Fig. 7a). Reduction of  $\text{Fe}^{3+}$  by  $\text{H}_2\text{O}_2$  happens during Fenton reaction initiation steps [11], which induces production  $\cdot\text{OH}$  radicals. In the period from 100 to 180 min the reaction rate is slower and proceeds at a steady level, which is common for heterogeneous Fenton reaction propagation and termination steps. Dye mineralization had a similar trend, where TOC removal increases over the period up to 80 min, while afterwards the reaction proceeds slowly (66.8 %). The difference in observed RB4 decolorization and mineralization is due to different reaction pathways. Additionally, dye sorption was generally steady and in the range from 35.1 to 49.3 %, pointing to the significance of the Fenton reaction. When methanol was added as an  $\cdot\text{OH}$  scavenger, ~50 % lower efficacy was obtained in the first 30 min. As the reaction proceeds, it is suspected that new radical species are formed [41], which further affect dye decolorization. The  $\cdot\text{OH}$  radical scavenging test was also implemented to determine  $\cdot\text{OH}$  radicals presence after 15 min, as it was assumed that the highest amount of radical species arises at that time. The identified capacity of 79.6 %, additionally confirms the Fenton reaction.

Finally, the acute toxicity test on *V. fischeri* bacteria was conducted (Fig. 7b) for all samples in the determined time range. The starting inhibition of the RB4 solution was 57.9 % (white point in the graph). The inhibition curve shows that RB4 intermediates are the most toxic in the first phase of the reaction (90.2 % up to 45 min). Afterwards, inhibition

greatly decreases to 22.4 % (180 min), thus presenting low toxicity to the non-selective bacteria. In a previous work [6], RB4 effluent after the Fenton process induced high toxicity (>95 %) due to detected polycyclic hydrocarbons and compounds that contained Cl atoms as degradation intermediates. It is assumed that similar compounds (with the inhibitory potential) are formed in the first 60 min, while during further reaction these compounds are degraded thus ensuring the sufficient effluent quality.

Under the optimal heterogeneous Fenton reaction conditions RB4 degradation products were analyzed by the GC-MS technique and detected compounds are presented in Table 5. Cyclic hydrocarbons, phthalates, organic acids and its esters, an organonitrogen compound, phenols and alcohols were identified by the NIST and AMDIS databases. It can be seen that the initial oxidation product of RB4 dye (1-amino-9,10-anthracenedione) was not found, which may be the evidence of molecule chromophore degradation by  $\cdot\text{OH}$  radicals to phthalates, phenols and organic acids [2,42]. Also, triazine compounds were not found, thus confirming dye mineralization during the reaction time.

Table 5. GC-MS list of degradation products

Retention time, min	CAS number	Compound Name	Molecular formula
5.63	91203	Naphthalene	$\text{C}_{10}\text{H}_8$
8.58	112425	1-Undecanol	$\text{C}_{11}\text{H}_{24}\text{O}$
9.07	96764	Phenol, 2,4-bis(1,1-dimethylethyl)-	$\text{C}_{14}\text{H}_{22}\text{O}$
9.38	90437	o-Hydroxybiphenyl	$\text{C}_{12}\text{H}_{10}\text{O}$
15.2	36653824	1-Hexadecanol	$\text{C}_{16}\text{H}_{34}\text{O}$
16.8	84695	1,2-Benzenedicarboxylic acid, bis(2-methylpropyl) ester	$\text{C}_{16}\text{H}_{22}\text{O}_4$
19.5	84742	Dibutyl phthalate	$\text{C}_{16}\text{H}_{22}\text{O}_4$
19.7	57103	n-Hexadecanoic acid	$\text{C}_{16}\text{H}_{32}\text{O}_2$
23.7	129000	Pyrene	$\text{C}_{16}\text{H}_{10}$
24.3	112629	9-Octadecenoic acid (Z)-, methyl ester	$\text{C}_{19}\text{H}_{36}\text{O}_2$
30.3	117817	Bis(2-ethylhexyl) phthalate	$\text{C}_{24}\text{H}_{38}\text{O}_4$
33.5	0	l-Proline, N-methoxycarbonyl-, heptadecyl ester	$\text{C}_{24}\text{H}_{45}\text{NO}_4$

### 3. 5. Fe-WSH reusability

Fe-WSH stability is expressed as a content of leached Fe. Under the optimal Fenton reaction conditions and during the first 60 min, only  $0.11 \text{ mg Fe dm}^{-3}$  was detected in the aqueous phase. Until 180 min,  $0.13 \text{ mg dm}^{-3}$  in total was leached amounting to only 0.02 % of the total Fe amount in the system ( $66.9 \text{ mg Fe}$  for  $100 \text{ mg Fe-WSH}$ , value obtained according to EDS analysis; Fig. 2), thus providing an insight in the high catalyst stability.

Additionally, a reusability test was performed (Fig. 8).

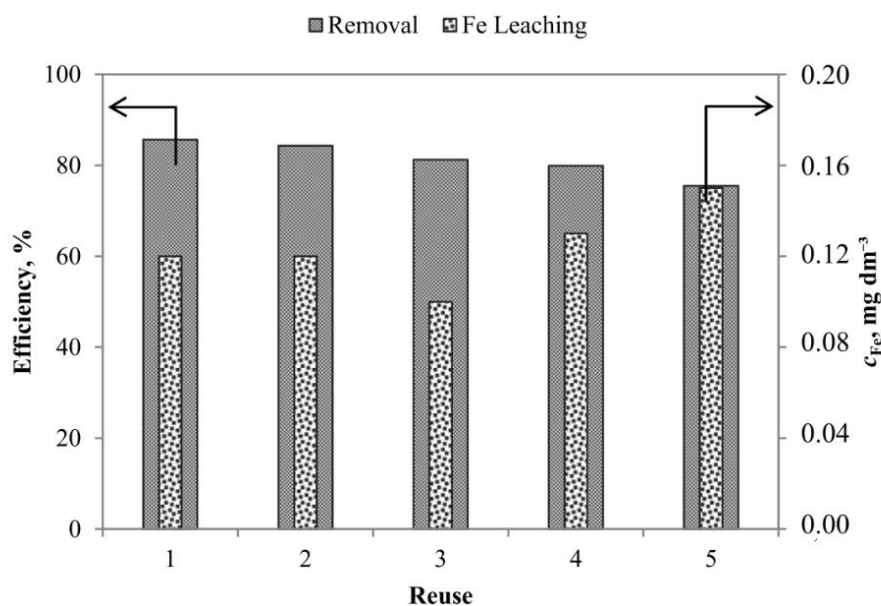


Fig. 8. Fe-WSH reusability test



The Fe-WSH activity loss over 5 runs was ~12 % (1<sup>st</sup> = 85.7; 5<sup>th</sup> = 75.5 %), while the total Fe leaching was constant (up to 0.15 mg dm<sup>-3</sup>). These results suggest that the catalyst has high physical-chemical stability. The reason for the observed efficiency reduction is due to possible adsorption of the dye and its intermediates, which were not completely removed by washing with DI water and at low temperature treatment. All presented results indicate that Fe-WSH is appropriate for effective synthetic dye degradation with long-term stability in acidic conditions.

#### 4. CONCLUSION

In the present work, waste soybean hulls (WSH) were investigated as a Fe-support in two forms: raw and carbonized in order to contribute to agricultural solid waste value-addition. Facile ultrasound improved impregnation was implemented in order to produce heterogeneous Fenton catalyst for dye degradation. Characterization of the initial and obtained materials demonstrated increase in the specific surface area due to decomposition of WSH constituents during carbonization in order to obtain biocarbon (BC) and during further thermal activation and impregnation to obtain Fe-enriched materials (*i.e.* Fe-WSH and Fe-BC), thus producing catalysts with high mesoporosity and hematite as active sites for Fenton reaction. Among the investigated materials, BC could be used as an adsorbent in alkaline media, while Fe-WSH showed greater ability for <sup>•</sup>OH production in acidic conditions. Next, the heterogeneous Fenton reaction conditions were optimized by using the RSM and CCD experiment design. The following reaction conditions were indicated by the reduced model: 3 mM H<sub>2</sub>O<sub>2</sub>, 100 mg Fe-WSH and the reaction time of 180 min, at constant pH 3, the RB4 concentration of 50 mg dm<sup>-3</sup> and at room temperature. The achieved dye removal and mineralization were 85.7 and 66.8 %, respectively, while the Fe-WSH catalyst showed high stability and reaction intermediates formed during the oxidation process had a low inhibitory effect on *Vibrio fischeri* bacteria. Lower oxidant demand and the possibilities for the catalyst reuse make the treatment more economical. For future use of the heterogeneous Fenton process in industrial wastewater treatment it is important to achieve the environmentally safe effluent with low toxicity and organic and inorganic loads. Likewise, cascading use of waste-originating catalysts (in wastewater treatment, construction, agriculture, etc.) should be enforced in design of circular economy systems.

**Acknowledgements:** The authors acknowledge the financial support of the Ministry of Education, Science and Technological Development of the Republic of Serbia [Grant No. 451-03-68/2020-14/200125] and the Science Fund of the Republic of Serbia [PROMIS – WasteWaterForce project (6066881)]. The authors also kindly thank a soybean processing company for providing raw SBH, PhD Goran Kitić and PhD Jovana Stanojev (Biosense Institute) for SEM/EDS analyses, PhD Srđan Rakić (Faculty of Sciences) for XRD analyses, and PhD Branko Kordić (Faculty of Sciences) for FTIR analyses.

#### REFERENCES

- [1] Holkar CR, Jadhav AJ, Pinjari DV, Mahamuni NM, Pandit AB. A critical review on textile wastewater treatments: Possible approaches. *J. Environ. Manage.* 2016; 182: 351–366. <https://dx.doi.org/10.1016/j.jenvman.2016.07.090>
- [2] Gözmen B, Kayan B, Gizir M, Heresnov A. Oxidative degradations of reactive blue 4 dye by different advanced oxidation methods. *J. Hazard. Mater.* 2009; 168: 129–136. <https://dx.doi.org/10.1016/j.jhazmat.2009.02.011>
- [3] Hassan H, Hameed BH. Fe-Natural Zeolite as Highly Active Heterogeneous Catalyst in Decolorization of Reactive Blue 4. *Int. J. Environ. Sci. Dev.* 2020; 11: 133–137. <https://dx.doi.org/10.18178/ijesd.2020.11.3.1239>
- [4] Fatma NY, Riyanti F, Hariani PL, Nurbaiti B. Synthesis of chitosan/alumina composite by sol gel method for adsorption of procion blue MX-R dye from wastewater songket industry. *J. Phys. Conf. Ser.* 2019; 1282: 012080. <https://doi.org/10.1088/1742-6596/1282/1/012080>
- [5] da Silva RG, de Andrade AR. Degradation of the Dye Reactive Blue 4 by Coupled Photoassisted Electrochemistry at DSA®-Type Electrode. *J. Brazil. Chem. Soc.* 2016; 27: 857–865. <http://dx.doi.org/10.5935/0103-5053.20150338>
- [6] Tomin MB, Kulic A, Kerkez D, Prica M, Rapajic S, Pilipovic DT, Pesic V. Reactive dye degradation using Fe-loaded bentonite as a Fenton-like catalyst: From process optimization to effluent acute toxicity. *Fresen. Environ. Bull.* 2017; 26: 8184–8198. [https://www.prt-parlar.de/download\\_feb\\_2017/](https://www.prt-parlar.de/download_feb_2017/)
- [7] Zhang M, Dong H, Zhao L, Wang D, Meng D. A review on Fenton process for organic wastewater treatment based on optimization perspective. *Sci. Total Environ.* 2019; 670: 110–121. <https://dx.doi.org/10.1016/j.scitotenv.2019.03.180>
- [8] Eloussaief M, Hamza W, Ghorbali G, Kallel N, Benzina M. Fe-Rich Aragonite Concretion Applied to Industrial Dye Purification Using Fenton and Photo-Fenton Technologies. *Waste Biomass Valori.* 2021; 12: 3303-3313. <https://dx.doi.org/10.1007/s12649-020-01228-6>

- [9] Wang N, Zheng T, Zhang G, Wang P. A review on Fenton-like processes for organic wastewater treatment. *J. Environ. Chem. Eng.* 2016; 4: 762–787. <https://dx.doi.org/10.1016/j.jece.2015.12.016>
- [10] Javaid R, Qazi UY. Catalytic oxidation process for the degradation of synthetic dyes: An overview. *Int. J. Environ. Res. Public Health.* 2019; 16: 2066. <https://dx.doi.org/10.3390/ijerph16112066>
- [11] Zhu Y, Zhu R, Xi Y, Zhu J, Zhu G, He H. Strategies for enhancing the heterogeneous Fenton catalytic reactivity: A review. *Appl. Catal. B Environ.* 2019; 255: 117739. <https://doi.org/10.1016/j.apcatb.2019.05.041>
- [12] Bello M, Raman AA, Asghar A. A review on approaches for addressing the limitations of Fenton oxidation for recalcitrant wastewater treatment. *Process Saf. Environ. Prot.* 2019; 126: 119-140. <https://doi.org/10.1016/j.psep.2019.03.028>
- [13] Nidheesh PV. Heterogeneous Fenton catalysts for the abatement of organic pollutants from aqueous solution: A review. *RSC Adv.* 2015; 5: 40552–40577. <https://dx.doi.org/10.1039/c5ra02023a>
- [14] Wang J, Bai Z. Fe-based catalysts for heterogeneous catalytic ozonation of emerging contaminants in water and wastewater. *Chem. Eng. J.* 2017; 312: 79–98. <https://dx.doi.org/10.1016/j.cej.2016.11.118>
- [15] Girish CR. Various impregnation methods used for the surface modification of the adsorbent: A review. *Int. J. Eng. Technol.* 2018; 7: 330–334. <https://dx.doi.org/10.14419/ijet.v7i4.7.20571>
- [16] Elías VR, Rodríguez PAO, Vaschetto EG, Pecchi GA, Huck-Iriart C, Casuscelli SG, Eimer GA. Tailoring the stability and photo-Fenton activity of Fe-modified nanostructured silicates by tuning the metal speciation from different synthesis conditions. *Mol. Catal.* 2020; 481: 110217. <https://dx.doi.org/10.1016/j.mcat.2018.10.012>
- [17] Setiawan WK, Chiang KY. Crop Residues as Potential Sustainable Precursors for Developing Silica Materials: A Review. *Waste Biomass Valori.* 2020; 2207-2236. <https://dx.doi.org/10.1007/s12649-020-01126-x>
- [18] Campbell-Johnston K, Vermeulen WJV, Reike D, Brulot S. The Circular Economy and Cascading: Towards a Framework. *Resour. Conserv. Recycl. X.* 2020; 7: 100038. <https://dx.doi.org/10.1016/j.rcrx.2020.100038>
- [19] Xiang W, Zhang X, Chen J, Zou W, He F, Hu X, Tsang DCW, Ok YS, Gao B. Biochar technology in wastewater treatment: A critical review. *Chemosphere.* 2020; 252: 126539. <https://dx.doi.org/10.1016/j.chemosphere.2020.126539>
- [20] Enaime G, Baçaoui A, Yaacoubi A, Lübken M. Biochar for wastewater treatment-conversion technologies and applications. *Appl. Sci.* 2020; 10: 3492. <https://dx.doi.org/10.3390/app10103492>
- [21] Pan X, Gu Z, Chen W, Li Q. Preparation of biochar and biochar composites and their application in a Fenton-like process for wastewater decontamination: A review. *Sci. Total Environ.* 2021; 754: 142104. <https://dx.doi.org/10.1016/j.scitotenv.2020.142104>
- [22] Statistical Office of the Republic of Serbia. Statistical Release PO16: Realized production of wheat and early fruit and expected yields of late crops, fruit and grapes, 2020. *Agric. Stat.* 2020; 262: 1-2. ISSN 0353-9555
- [23] Barros PJR, Ascheri DPR, Santos MLS, Morais CC, Ascheri JLR, Signini R, dos Santos DM, de Campos AJ, Devilla IA. Soybean hulls: Optimization of the pulping and bleaching processes and carboxymethyl cellulose synthesis. *Int. J. Biol. Macromol.* 2020; 144: 208–218. <https://dx.doi.org/10.1016/j.ijbiomac.2019.12.074>
- [24] Liu H-M, Li H-Y. Application and Conversion of Soybean Hulls. In: Kasai M, ed. *Soybean - The Basis of Yield, Biomass and Productivity*. IntechOpen; 2017: 111–132. <https://dx.doi.org/10.5772/66744>
- [25] Qing Q, Guo Q, Zhou L, Gao X, Lu X, Zhang Y. Comparison of alkaline and acid pretreatments for enzymatic hydrolysis of soybean hull and soybean straw to produce fermentable sugars. *Ind. Crops Prod.* 2017; 109: 391–397. <https://dx.doi.org/10.1016/j.indcrop.2017.08.051>
- [26] Neto WPF, Silvério HA, Dantas NO, Pasquini D. Extraction and characterization of cellulose nanocrystals from agro-industrial residue - Soy hulls. *Ind. Crops Prod.* 2013; 42: 480–488. <https://dx.doi.org/10.1016/j.indcrop.2012.06.041>
- [27] Toro-Trochez JL, Carrillo-Pedraza ES, Bustos-Martínez D, García-Mateos FJ, Ruiz-Rosas RR, Rodríguez-Mirasol J, Cordero T. Thermogravimetric characterization and pyrolysis of soybean hulls. *Bioresour. Technol. Reports.* 2019; 6: 183–189. <https://dx.doi.org/10.1016/j.biteb.2019.02.009>
- [28] Herde ZD, Dharmasena R, Sumanasekera G, Tumuluru JS, Satyavolu J. Impact of hydrolysis on surface area and energy storage applications of activated carbons produced from corn fiber and soy hulls. *Carbon Resour. Convers.* 2020; 3: 19–28. <https://dx.doi.org/10.1016/j.crcon.2019.12.002>
- [29] Bečelić-Tomin M, Kulić A, Kerkez Đ, Pilipović DT, Pešić V, Dalmacija B. Synthesis of impregnated bentonite using ultrasound waves for application in the Fenton process. *Clay Miner.* 2018; 53: 203–212. <https://dx.doi.org/10.1180/clm.2018.14>
- [30] Xiao C, Li J, Zhang G. Synthesis of stable burger-like  $\alpha$ -Fe<sub>2</sub>O<sub>3</sub> catalysts: Formation mechanism and excellent photo-Fenton catalytic performance. *J. Clean. Prod.* 2018; 180: 550–559. <https://dx.doi.org/10.1016/j.jclepro.2018.01.127>
- [31] Trovó AG, Nogueira RFP, Agüera A, Fernandez-Alba AR, Malato S. Degradation of the antibiotic amoxicillin by photo-Fenton process - Chemical and toxicological assessment. *Water Res.* 2011; 45: 1394–1402. <https://dx.doi.org/10.1016/j.watres.2010.10.029>
- [32] Milidrag GP, Prica M, Kerkez D, Dalmacija B, Kulic A, Pilipovic DT, Tomin MB. A comparative study of the decolorization capacity of the solar-assisted Fenton process using ferrioxalate and Al, Fe-bentonite catalysts in a parabolic trough reactor. *J. Taiwan Inst. Chem. Eng.* 2018; 93: 436–449. <https://dx.doi.org/10.1016/j.jtice.2018.08.015>
- [33] Balint T, Chang BP, Mohanty AK, Misra M. Underutilized Agricultural Co-Product as a Sustainable Biofiller for Polyamide 6,6: Effect of Carbonization Temperature. *Molecules.* 2020; 25: 1455. <https://dx.doi.org/doi:10.3390/molecules25061455>

- [34] Wu Q, Ouyang J, Xie K, Sun L, Wang M, Lin C. Ultrasound-assisted synthesis and visible-light-driven photocatalytic activity of Fe-incorporated TiO<sub>2</sub> nanotube array photocatalysts. *J. Hazard. Mater.* 2012; 199–200: 410–417. <https://dx.doi.org/10.1016/j.jhazmat.2011.11.031>
- [35] Nandiyanto ABD, Oktiani R, Ragadhita R. How to read and interpret ftir spectroscopy of organic material. *Indones. J. Sci. Technol.* 2019; 4: 97–118. <https://dx.doi.org/10.17509/ijost.v4i1.15806>
- [36] Chen Y, Shi J, Du Q, Zhang H, Cui Y. Antibiotic removal by agricultural waste biochars with different forms of iron oxide. *RSC Adv.* 2019; 9: 14143–14153. <https://dx.doi.org/10.1039/c9ra01271k>
- [37] Wang QJ, Liu RJ, Shen XQ, Wu DM, Li HH. Fabrication and methyl blue adsorption kinetics of  $\alpha$ -Fe<sub>2</sub>O<sub>3</sub> nanotubes by electrospinning. *Adv. Mater. Res.* 2013; 699: 302–307. <https://dx.doi.org/10.4028/www.scientific.net/AMR.699.302>
- [38] Galan J, Trilleras J, Zapata PA, Arana VA, Grande-Tovar CD. Optimization of chitosan glutaraldehyde-cross linked beads for reactive blue 4 anionic dye removal using a surface response methodology. *Life.* 2021; 11: 1–20. <https://dx.doi.org/10.3390/life11020085>
- [39] Zhao L, Lin ZR, Ma XH, Dong, YH. Catalytic activity of different iron oxides: Insight from pollutant degradation and hydroxyl radical formation in heterogeneous Fenton-like systems. *Chem. Eng. J.* 2018; 352: 343–351. <https://dx.doi.org/10.1016/j.cej.2018.07.035>
- [40] Becelic-Tomin M, Dalmacija B, Rajic L, Tomasevic D, Kerkez D, Watson M, Prica M. Degradation of anthraquinone dye reactive blue 4 in pyrite ash catalyzed fenton reaction. *Sci. World J.* 2014; 234654. <https://dx.doi.org/10.1155/2014/234654>
- [41] Schneider JT, Firak DS, Ribeiro RR, Peralta-Zamora P. Use of scavenger agents in heterogeneous photocatalysis: truths, half-truths, and misinterpretations. *Phys. Chem. Chem. Phys.* 2020; 22: 15723–15733. <https://dx.doi.org/10.1039/d0cp02411b>
- [42] Stupar SL, Grgur BN, Radišić MM, Onjia AE, Ivanković ND, Tomašević AV, Mijin D. Oxidative degradation of Acid Blue 111 by electro-assisted Fenton process. *J. Water Process Eng.* 2020; 36: 101394. <https://dx.doi.org/10.1016/j.jwpe.2020.101394>

## SAŽETAK

### Primena impregnisanog biouglja proizvedenog iz sojinih ljuspica u procesu obezbojavanja boje

Aleksandra Kulić Mandić, Milena Bečelić-Tomin, Gordana Pucar Milidrag, Milena Rašeta i Đurđa Kerkez

*Prirodno-matematički fakultet, Univerzitet u Novom Sadu, Departman za hemiju, biohemiju i zaštitu životne sredine, 21000 Novi Sad, Srbija*

(Naučni rad)

U cilju moguće valorizacije, otpadne sojine ljuspice (engl. *waste soybean hulls*, OSLj) su ispitivane kao nosači jona Fe, u dve različite forme: sirovoy i karbonizovanoj (engl. *biocarbon*, BU). Impregnacija jonima Fe(III) je implementirana radi sinteze heterogenih Fenton katalizatora (Fe-OSLj i Fe-BU) za obezbojavanje vodenog rastvora *Reactive Blue 4* (RB4) boje. Karakterizacija materijala je pokazala porast specifične površine zbog dekompozicije konstituenata OSLj tokom karbonizacije (prilikom dobijanja BU) i termalne aktivacije (prilikom dobijanja Fe-OSLj i Fe-BU), gde su dobijeni katalizatori visoke mezoporoznosti sa hematitom kao aktivnom fazom za odvijanje Fentonove reakcije. Među pripremljenim materijalima, Fe-OSLj je pokazao značajnu sposobnost produkcije •OH radikala u kiseloy sredini. Dalje, optimizacija heterogenog Fenton procesa je izvedena primenom metodologije odzivnih površina (engl. *Respose Surface Methodology*, RSM), gde su redukovanim modelom izdvojeni sledeći uslovi reakcije: 3 mM H<sub>2</sub>O<sub>2</sub>, 100 mg Fe-OSLj, vreme reakcije od 180 min, pri konstantnim vrednostima pH = 3, koncentracije boje od 50 mg RB4 dm<sup>-3</sup> i na sobnoj temperaturi. Postignuto je 88,7% i 66,8% obezbojavanja i mineralizacije RB4 boje, redom; Fe-OSLj je pokazao veliku stabilnost, a reakcioni intermedijeri formirani tokom oksidacionog procesa su imali nizak inhibitorni efekat na *Vibrio fischeri* bakterije.

*Ključne reči:* valorizacija; Fe(III)-impregnacija; metoda odzivnih površina; Reactive Blue 4; ponovna upotreba